NANO LETTERS

Letter

pubs.acs.org/NanoLett

Too Hot for Photon-Assisted Transport: Hot-Electrons Dominate Conductance Enhancement in Illuminated Single-Molecule Junctions

E-Dean Fung,[†] Olgun Adak,[†] Giacomo Lovat,[†] Diego Scarabelli,[†] and Latha Venkataraman*[,†,‡]

[†]Department of Applied Physics and Applied Mathematics and [‡]Department of Chemistry, Columbia University, New York, New York 10027, United States

Supporting Information

ABSTRACT: We investigate light-induced conductance enhancement in single-molecule junctions via photon-assisted transport and hot-electron transport. Using 4,4′-bipyridine bound to Au electrodes as a prototypical single-molecule junction, we report a 20−40% enhancement in conductance under illumination with 980 nm wavelength radiation. We probe the effects of subtle changes in the transmission function on light-enhanced current and show that discrete variations in the binding geometry result in a 10% change in enhancement. Importantly, we prove theoretically that the steady-state behavior of photon-assisted transport and hot-electron transport is identical but that hot-electron transport is the dominant mechanism for optically induced conductance enhancement in single-molecule junctions when the wavelength used is absorbed by the electrodes and the hot-electron relaxation time is long. We confirm this experimentally by performing polarization-dependent conductance measurements of illuminated 4,4′-bipyridine junctions. Finally, we perform lock-in type measurements of optical current and conclude that currents due to laser-induced thermal expansion mask optical currents. This work provides a robust experimental framework for studying mechanisms of light-enhanced transport in single-molecule junctions and offers tools for tuning the performance of organic optoelectronic devices by analyzing detailed transport properties of the molecules involved.

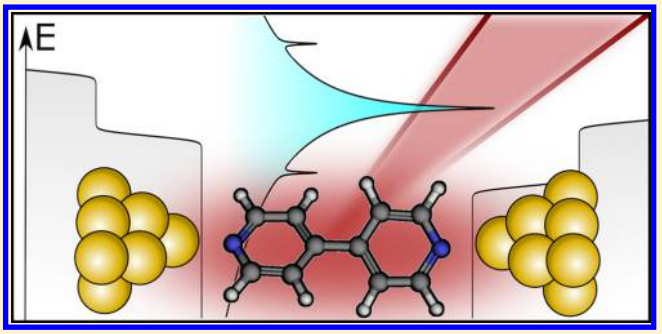

KEYWORDS: *Photon-assisted transport, hot-electron, single-molecule, Tien-Gordon, surface plasmon*

The ability to control charge transport across single-molecule devices using light would provide an important break-through toward the expansion of functionality at the nanometer scale.[1−4] Theoretical studies have predicted that the conductance of a single molecule could be enhanced upon illumination via a mechanism commonly referred to as photon-assisted transport (PAT).[5−8] PAT was first observed in superconductors under microwave radiation,[9,10] but the photon flux necessary to observe PAT in single-molecule junctions is often much larger than what can be achieved using traditional diffraction-limited optics. However, with recent advances in photonics electromagnetic fields can be concentrated into subdiffraction-limited volumes by coupling the fields to the localized surface plasmons resonances of metal nanostructures, making it possible to observe light-enhanced charge transport through molecular systems.[11−16]

Several pioneering experiments have attributed optically induced current enhancements in tunnel junctions,[17−21] gold point-contacts,[22−24] and, more recently, molecular junctions[25−27] to PAT. However, theoretical[28−31] and experimental[32−35] studies have shown that the same localized surface plasmons that confine light around nanostructures also give rise to populations of hot-electrons. Despite strong interest in both phenomena, there has been little discussion of the relationship between PAT and hot-electron transport,[36] and it is often assumed that all observed optical signatures are due to one effect or the other. Furthermore, studies of PAT in single-molecule systems either have stringent fabrication requirements[27] or do not reliably couple light into the junction.[25]

Previous works have shown that scanning tunneling microscopes can be used to effectively couple photons into single-molecule junctions.[37,38] In this study, we utilize a similar system which permits polarization-dependent measurement of light-induced conductance enhancement over thousands of junctions. By taking advantage of detailed knowledge of the transport properties of 4,4′-bipyridine (BP) in an Au-molecule−Au junction,[39,40] we experimentally probe the relationship between the molecular junction and light-induced enhancement. We then use a Landauer-like model to show that PAT and hot-electron transport have equivalent steady-state current signatures. A straightforward calculation shows that hot-electron transport constitutes the majority of light-induced enhancement in conductance, which we validate experimentally. Finally, we show that techniques that rely on modulating the light intensity at low frequencies (<GHz) cannot be applied

Received: December 7, 2016
Revised: January 19, 2017
Published: January 23, 2017

DOI: 10.1021/acs.nanolett.6b05091
Nano Lett. 2017, 17, 1255−1261

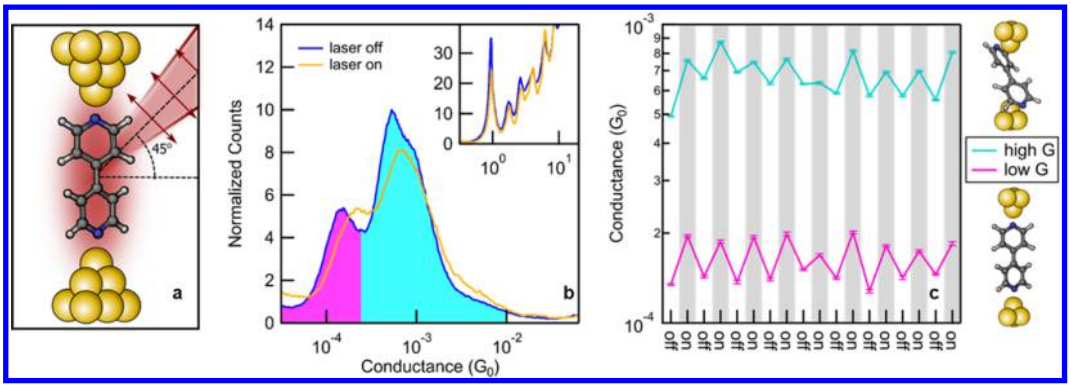

Figure 1. (a) Schematic of an illuminated metal-molecule-metal junction with 4,4′-bipyridine (BP) in the low-conducting geometry. Arrows indicate the direction of polarization. (b) Logarithmically binned 1D conductance histograms of BP junctions at 180 mV bias for dark (laser off) and illuminated (laser on) junctions, normalized to the total number of junctions. Inset shows the high-conductance region for the same histograms. The high (low) conductance peak is shaded in teal (magenta). (c) A series of conductance measurements where the laser is successively turned on and off. Each point represents peak positions in a conductance histogram constructed from 500 traces. Error bars represent the standard error of the fit. Binding geometry of high- and low-conductance configurations are depicted on the right.

to these systems as thermal expansion effects will mask any optical current.

We employed the scanning tunneling microscope break junction (STM-BJ) method described in previous works[41] to characterize the electronic properties of BP in a metal−molecule−metal contact geometry. We formed Au tips by crimping Au wire with cutting pliers and used substrates made by thermally evaporating approximately 100 nm of Au onto mica sheets on steel pucks. After thermally evaporating BP onto the substrate, we heated the substrate to 100 °C for approximately 5 min to decrease the density of BP on the surface. This additional procedure reduces the probability of forming multimolecule junctions. We illuminated the junction by focusing a 980 nm continuous-wave laser (Thorlabs, Inc.) at the junction using a 50× microscope objective with numerical aperture 0.42 and a working distance of 17 mm (Mitutoyo). The beam was angled at 45 ± 2° with respect to the substrate and polarized parallel to the plane of incidence, as shown in Figure 1a. We operate the laser diode at around 100 mW and estimate the peak intensity at the junction to be 2000−6000 kW·cm^{-2}.

For each measurement, the Au tip was brought into contact with the substrate until a conductance greater than 2 G_0 was achieved, where $G_0 = 2e^2/h$ is the quantum of conductance. The tip was then withdrawn at a velocity of 18 nm/s, during which time conductance was measured as a function of tip/sample displacement. Individual conductance traces show characteristic plateaus at decreasing integer multiples of G_0 as the displacement increases. In addition, traces for BP typically show two molecular plateaus at around 5.6×10^{-4} G_0 and 1.3×10^{-4} G_0. The exact conductance peak values depend to some extent on the molecule concentration[42] and are therefore slightly different from past works. The high- and low-conducting BP junctions are attributed to two different molecular binding geometries as has been discussed in detail before.[39] Thousands of individual conductance traces were measured under ambient conditions, from which statistically relevant conductance information can be extracted.

We conducted STM-BJ measurements on BP with and without laser illumination at a bias of 180 mV. In order to account for any potential time dependence, we switched the laser on or off every 500 measurements. The experiment was paused for 10 min every time the laser was switched on (off) to allow the tip to expand (contract) and reach steady-state temperature. We combined nine sets of 500 traces to create the one-dimensional (1D) conductance histograms shown in Figure 1b. Each histogram was created from 4500 conductance-displacement traces collected without data selection, logarithmically binned in units of G_0, and normalized to the number of traces represented. Both histograms show the two conductance peaks, one high and one low, characteristic of Au−BP−Au junctions. It is immediately apparent that the conductance peaks for junctions under illumination (orange) are shifted with respect to those of junctions without illumination (blue). By fitting each histogram in Figure 1b with a double Lorentzian curve, we extracted the most probable conductance of a BP junction in either a high-conducting (teal-filled) or low-conducting (magenta-filled) configuration. Comparing the most probable conductance of dark and illuminated junctions, we obtain a 27% and 33% enhancement in conductance for high- and low-conductance peaks, respectively.

Figure 1c shows the evolution of the high and low peak-conductance values at 180 mV bias as the laser is switched on and off, each point representing the fitted peaks in a conductance histogram created from 500 individual traces. The conductance is clearly modulated by near-infrared illumination. The observed conductance enhancement and switching behavior is reproducible with multiple tip and sample pairs, although the actual conductance enhancement varies between experiments because of variations in tip shape and alignment. Across all experiments, however, the enhancement observed in low-conducting peaks is always higher than that observed in high-conducting peaks with enhancements of up to 60% in low-conducting junctions. Additionally, we observe a small enhancement of around 1% in the 1 G_0 conductance peak, which is consistent with past reports.[22,34]

Before considering any conductance enhancement mechanisms unique to light, we must rule out mechanisms pertaining to thermal effects under illumination that might explain the enhanced conductance. We first consider the impact of an increase in the electrode equilibrium temperature due to laser heating. To estimate the electrode temperature under illumination, we performed STM-BJ measurements on BP junctions while heating the substrate up to 110 °C using a resistive heating element. Above 110 °C, we did not observe

DOI: 10.1021/acs.nanolett.6b05091
Nano Lett. 2017, 17, 1255−1261

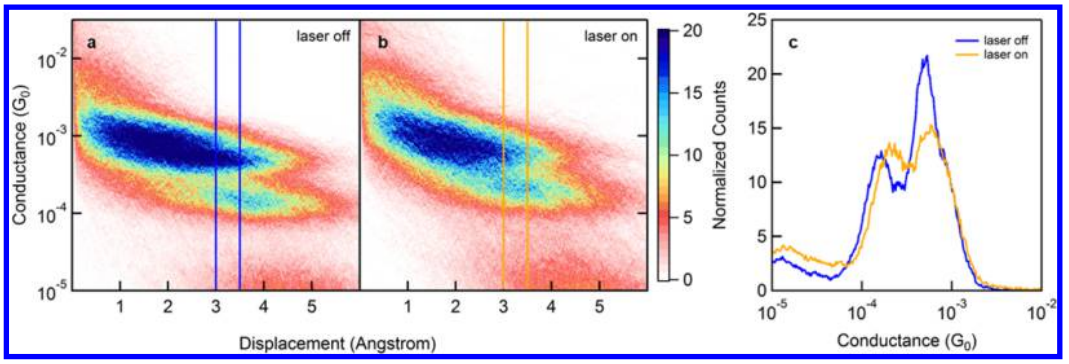

Figure 2. Two-dimensional conductance-displacement histograms of BP measured (a) without and (b) with illumination. Vertical lines delimit the range of displacement values used to construct (c), a 1D conductance histogram, normalized to the total number of points collected in the range of selected displacement values. The shift in Figure 1b is preserved under this analysis.

clear conductance peaks because BP desorbs from the substrate at that temperature. This places an upper bound on the temperature in the illuminated junctions. Additionally, heating decreases the height of the conductance peak at 1 G_0, similar to what we observe under illumination (see inset of Figure 1b). This is a result of increased mechanical instability of the Au point-contact.[43,44] Using the average number of points around the 1 G_0 peak in a single trace as a rough gauge of temperature, we estimate that the junction is heated to about 45 °C under illumination. More importantly, we find that the conductance does not change with temperature (see Supporting Information (SI) Figures S2c,d). We conclude, therefore, that the increase in temperature cannot account for the conductance enhancement observed under illumination.

Second, we briefly consider the impact of a temperature differential between the two electrodes, either due to the spatial profile of the beam cross-section or to geometric differences between the tip and substrate that may give rise to thermoelectric current. Thermopower measurements of BP at temperature gradients of up to 27 °C produce around 20 pA of thermoelectric currents.[45] This is approximately 100 times smaller than the typical currents in BP junctions under 180 mV bias. As a result, the contribution of thermal gradients to the current enhancement seen in Figure 1b can safely be neglected.

Next, we explore the impact of electrode separation on the measured conductance enhancement. In each conductance trace, we defined zero displacement as the position where the conductance falls below 0.5 G_0, corresponding to where the Au−Au junction was broken. We created two-dimensional (2D) conductance-displacement histograms of the data presented in Figure 1b by simultaneously binning each data point with respect to conductance and displacement. These are shown in Figure 2a,b for dark and illuminated junctions, respectively. In both histograms, we again see the two characteristic conductances with the low-conductance geometry only occurring after the junction has been extended by around 2 Å. When the laser is on, we make two observations. First, the high-conductance plateaus are on average shorter by almost 0.5 Å and there are more junctions that form low-conductance traces, as indicated by the color scale. Second, the junctions break to noise much sooner, as evidenced by the early onset of the noise floor. We attribute these phenomena to the aforementioned decrease in junction lifetimes owing to the raised temperature.

Because the conductance of BP is inversely proportional to electrode separation, it is important to check that the shifts upon illumination are not due to selection bias against more extended (less conducting) junctions. To this end, we constructed conductance histograms shown in Figure 2c by considering only data points that are measured at a junction separation between 3 and 3.5 Å, depicted by the vertical lines in the 2D histograms (Figure 2a,b). The histograms in Figure 2c are normalized to the total number of points falling within the specified range. Fitting these histograms to double Lorentzian functions returns an enhancement in conductance of 14% and 34% for high- and low-conductance peaks, respectively, accentuating the difference in enhancement between the different binding geometries of BP. This rules out the possibility that the observed enhancement in illuminated junctions is merely due to selection bias against low-conducting junctions.

We now turn to an explanation of the conductance enhancement seen in Figure 1b in terms of a Landauer-like model of electron transport. In this model, current through a junction under an externally applied bias voltage without illumination is written as[46,47]

$$I_D[V, T(E)] = \frac{G_0}{e}\int_{-\infty}^{\infty} T(E)\left[f_L\left(E + \frac{eV}{2}\right) - f_R\left(E - \frac{eV}{2}\right)\right]dE \quad (1)$$

where I_D is the dark current, V is the applied bias voltage, f_L and f_R are the equilibrium Fermi distributions of left and right electrodes, respectively, and $T(E)$ is the junction transmission function. The energy E is referenced to the Fermi energy of the electrodes. The dark current is a function of the applied bias and the transmission function with a modest temperature dependence through the Fermi function.

For junctions under illumination, we must consider two main changes to eq 1. First, electronic states in the molecule interact with the electromagnetic field, resulting in a modified transmission function $T'(E)$. The time-averaged current through the junction is obtained by substituting eq 2 into eq 1, where V_{opt} is the amplitude of the alternating voltage generated across the junction by the light, J_n denotes the nth order Bessel function of the first kind, and $\hbar\omega$ is the photon energy.[5,7]

$$T'(E) = \sum_{n=-\infty}^{\infty} J_n^2\left(\frac{eV_{opt}}{\hbar\omega}\right)T(E + n\hbar\omega) \quad (2)$$

The modified transmission function is simply a sum of the original transmission function shifted by integer multiples of $\hbar\omega$. The square of the Bessel function gives the probability of absorbing or emitting n photons, and the transmission function

DOI: 10.1021/acs.nanolett.6b05091
Nano Lett. 2017, 17, 1255−1261

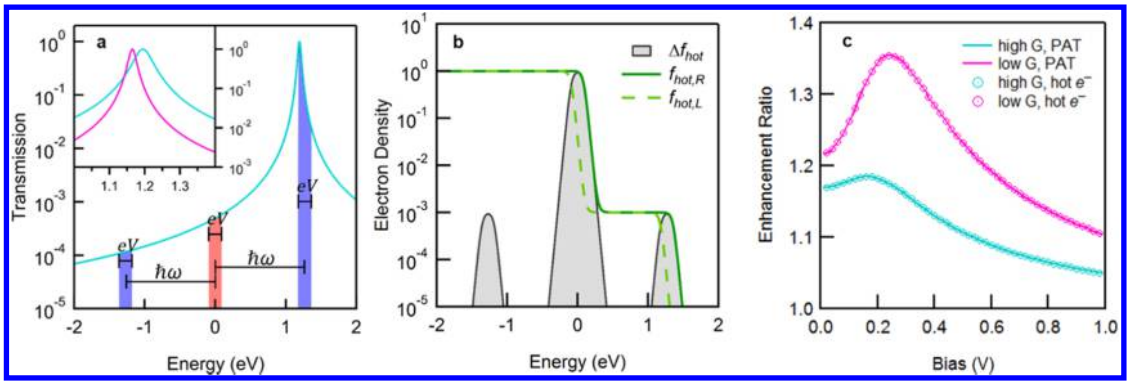

Figure 3. (a) Calculated transmission function of the high-conducting configuration of BP on a semilog plot. The additional current from photon-assisted tunneling is proportional to the blue area less twice the red area. The inset compares the transmission functions of high-conducting (teal) and low-conducting (magenta) BP junctions. Energy is referenced to the Fermi energy of the electrodes. (b) The computed hot-electron distribution for the right (solid-green) and left (dashed-green) electrodes for $\Delta\rho_0 = 10^{-3}$ and junction bias of 180 mV. The difference is the shaded area. (c) Calculated enhancement ratios as a function of bias using the transmission function of high-conducting (teal) and low-conducting (magenta) BP junctions. Solid curves were calculated using only photon-assisted tunneling; circular markers were calculated using only hot electron distributions. These curves cannot be distinguished.

in each term of the sum is shifted to account for the new energy of the tunneling electron. When the field intensity is small such that $eV_{opt} \ll \hbar\omega$, multiple-photon absorption and emission processes ($|n| > 1$) can be neglected. The modified transmission function can then be expanded to second order in $eV_{opt}/\hbar\omega$ and rewritten as the original transmission function plus a term proportional to the light intensity.

$$T'(E) \approx T(E) + \frac{1}{4}\left(\frac{eV_{opt}}{\hbar\omega}\right)^2 [T(E+\hbar\omega) + T(E-\hbar\omega) - 2T(E)] \tag{3}$$

The modification of the transmission function represents the PAT discussed in the introduction and is often attributed to the work of Tien and Gordon.[10] The Tien–Gordon model assumes that PAT is an adiabatic process and that the interaction between the electrons and the electromagnetic field occurs only in the bridge and not in the leads.[1,5,48] Because the HOMO–LUMO gap of BP is much larger than the photon energy[49,50] and the frequency used in this experiment is smaller than the plasma frequency of gold, we expect this model to qualitatively capture the steady-state behavior of PAT.

The second modification to the transport model under illumination pertains to the electron distributions in the leads. As noted before, the steady-state temperature in the leads is raised under illumination, which changes the Fermi distribution slightly. More importantly, electrons in the leads can absorb photons, which results in transient nonequilibrium electron distributions that decay via electron–electron interactions and electron–phonon coupling.[51,52] The time required for these so-called hot-electron distributions to thermalize into equilibrium Fermi distributions is around 500 fs,[53,54] at least an order of magnitude longer than the charge transfer time across a pyridine/gold interface.[55] We argue, therefore, that the Fermi distributions in eq 1 should be replaced with the non-equilibrium hot-electron distribution f_{hot} given in eq 4,[54] where f' denotes the equilibrium Fermi distribution for a slightly elevated temperature and $\Delta\rho_0$ is a constant proportional to the intensity of the illumination. Like $T'(E)$ for PAT, f_{hot} is the original Fermi-distribution plus a term proportional to the light intensity such that f_{hot} reduces to the Fermi-distribution in the limit that the light intensity goes to zero. This substitution is similar to those performed in recent works.[33,34]

$$f_{hot}(E) = f'(E) + \Delta\rho_0(V_{opt}^2)\{[1-f'(E)]f'(E-\hbar\omega) - f'(E)[1-f'(E+\hbar\omega)]\} \tag{4}$$

In order to understand how PAT and hot-electron distributions enhance the current in BP, we consider the two mechanisms separately. On the basis of theoretical and experimental work, the transmission function for BP junctions is well approximated by a single Lorentzian function given in eq 5, where ε is the alignment of the frontier molecular orbital from the Fermi level of the electrodes and Γ is the energy-independent broadening of the molecular resonance coupled to the electrodes.[56]

$$T(E) = \frac{\Gamma^2}{(E-\varepsilon)^2 + \Gamma^2} \tag{5}$$

The transmission function for high-conducting BP junctions is given by the teal curve in Figure 3a. If we approximate the Fermi distribution with a step function, the additional current due to PAT alone is proportional to the blue area less twice the red area. It is apparent from Figure 3a that for a given applied bias, the optical current is maximum when $\hbar\omega = \varepsilon$. For the high-conducting configuration of BP junctions, ε is measured to be 1.2 eV, justifying our choice of wavelength, which has photon energy 1.27 eV.[40]

Now we determine the effect of the hot-electron distribution without PAT. Figure 3b provides the calculated hot-electron distribution for the left and right electrodes, assuming $\Delta\rho_0 = 10^{-3}$ and a junction bias of 180 mV. Taking the difference reveals that the overall effect of the hot-electron distribution is to sample the transmission function above and below the Fermi level in much the same manner as PAT. Indeed, if $\Delta\rho_0 = (eV_{opt}/2\hbar\omega)^2$, we expect the current enhancement arising purely from the hot electrons to be indistinguishable from current enhancement due to PAT (assuming equilibrium Fermi distributions).

To show this explicitly, we computed the current enhancement ratio I_{opt}/I_D as a function of bias for both high- and low-conducting junctions (Figure 3c), where the current in illuminated junctions I_{opt} is calculated in two ways. We first assumed that the enhancement is due purely to PAT, substituting eq 3 into eq 1 and using equilibrium Fermi

DOI: 10.1021/acs.nanolett.6b05091
Nano Lett. 2017, 17, 1255–1261

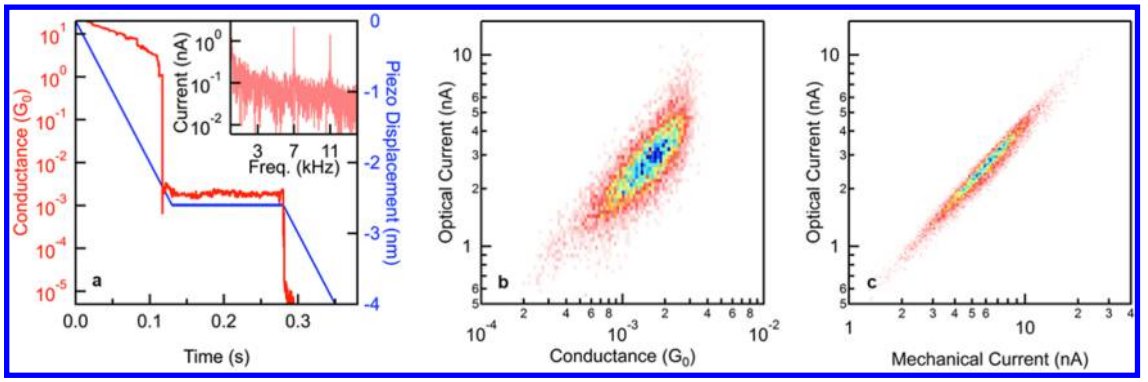

Figure 4. (a) Conductance and piezo displacement trace for a single high-conducting junction. Inset displays Fourier transform of current with peaks at 7 and 11 kHz corresponding to the mechanical and laser power modulation, respectively. (b) A 2D optical current versus conductance histogram of 10 000 BP junctions. (c) A 2D optical current versus mechanical current histograms of the same data in (b). Strong correlation suggests a shared mechanism.

distributions at an elevated temperature. A V_{opt} of 50 mV returns values consistent with our experiment. The computed enhancement ratio is higher for low-conducting junctions than for high-conducting junctions at all biases, completely consistent with our experimental results. We show in the SI that this is predominantly a consequence of the smaller coupling, Γ, in low-conducting junctions. Second, we computed the enhancement ratio using only hot-electron distributions, substituting the Fermi distributions in eq 1 with eq 4 without changing the transmission function to calculate I_{opt}. For a direct comparison with PAT, we chose $\Delta\rho_0 = (eV_{opt}/2\hbar\omega)^2$. As demonstrated by the circular markers in Figure 3c, the effect of hot electrons on transport is indistinguishable from the time-averaged effects of PAT. A more formal argument is provided in the SI. Thus, measurements of time-averaged transport under illumination cannot be used to distinguish between hot-electron transfer and PAT. It is necessary, therefore, to estimate the relative contributions of PAT and hot-electron distributions.

To this end, we estimated $\Delta\rho_0$ in terms of the absorption coefficient α, the hot-electron relaxation time τ, the density of states g, the electron−phonon mean free path λ, and the electrode separation distance d in eq 6 below. c, ϵ_0, and e are speed of light, free space permittivity, and elementary charge, respectively. Plugging in values from previous experiments[53,57−60] into eq 6 shows that the effect of hot-electron distributions is more than 100 times that of PAT.

$$\Delta\rho_0 = \frac{\alpha\tau c\epsilon_0}{2g\lambda e^2 d^2}\left(\frac{eV_{opt}}{\hbar\omega}\right)^2 \approx 36\left(\frac{eV_{opt}}{\hbar\omega}\right)^2 \quad (6)$$

To see if this is indeed an accurate estimate for $\Delta\rho_0$, we carried out the same experiments but with the laser polarization rotated to be orthogonal to the junction axis (parallel to the substrate). In Figure S7 of the SI, we show conductance histograms measured under this configuration where we clearly observe a conductance enhancement, albeit reduced. This is explained by a reduced plasmonic field enhancement, which is minimized when the polarization is perpendicular to the junction direction. Because the electric field must be parallel to the junction axis for photon-assisted transport to occur, the observed enhancement must be due to hot-electron distributions.

Having established that a simple STM-BJ setup is capable of measuring light-induced enhancement in conductance of BP metal−molecule−metal junctions, we explore lock-in techniques within this framework where the power of the laser is modulated at a specific frequency.[19,20,22,33] Currents that are modulated at the same frequency are measured using lock-in techniques and can be attributed to the laser light. However, ascribing the modulated currents to either PAT or hot-electron transport is complicated by thermal expansion. As the electrodes absorb photons, their temperature increases, resulting in thermal expansion.[61,62] This decreases the junction gap, which in turn increases the tunneling current. Thus, thermal expansion introduces an additional mechanism by which the current in the junction is modulated at the light modulation frequency, which must be decoupled from mechanisms uniquely induced by light.

Figure 4a illustrates the modified STM-BJ technique used to perform lock-in measurements. Instead of pulling the junction continuously, the piezoelectric positioner was stopped and held for 150 ms under an applied bias of 450 mV upon breaking the Au point-contact. During this hold segment, the stage was modulated at 7 kHz with an amplitude of 0.1 Å to mimic thermal expansion. The laser power was modulated at 11 kHz throughout the experiment by directly modulating the laser current source. However, because the junction can only sustain up to 2 Å of mechanical modulation before either breaking or forming gold point-contacts, we reduce the peak laser intensity by at least a factor of 2. The currents at the two modulation frequencies were extracted from a Fourier transform of the measured current, as shown in the inset. We will refer to the current at 7 kHz as mechanical current and the current at 11 kHz as optical current.

A 2D histogram of optical current against conductance representing over 10,000 traces is displayed in Figure 4b. We observe a linear dependence of optical current on the average conductance of the junction. Crucially, the measured optical currents are at least 100 times higher than predicted by our model, suggesting that the bulk of the current is due to a thermally induced mechanical modulation of the junction. As confirmation, we plotted a 2D histogram of optical current against mechanical current in Figure 2c. The strong correlation between the optical and mechanical current (correlation factor = 0.98) indicates a shared mechanism for modulation, namely changes in electrode separation. This result was also reproduced in tunnel junctions and gold point-contacts, as well as under different wavelengths of illumination (see SI).

We conclude that measurement techniques that rely on modulating the light intensity can only yield unambiguous

DOI: 10.1021/acs.nanolett.6b05091
Nano Lett. 2017, 17, 1255−1261

results when the absorption of the selected wavelength by the electrodes is negligible. Studies that use electromagnetic waves in the terahertz spectrum take advantage of this scenario.[27] Furthermore, we have demonstrated that investigations of PAT must be performed under conditions where the lifetime of hot-electrons is much shorter than the charge transfer time (which is inversely proportional to the coupling Γ) or where no hot-electron distributions are created, motivating further studies in the terahertz spectrum.

We have shown that the conductance of a single molecule junction can be enhanced under near-infrared radiation and find that the enhancement is predominantly due to hot-electron transport. Furthermore, the different binding geometries of 4,4′-bipyridine also reveal how subtle changes in the transmission function affect hot-electron transport, establishing some basic rules for designing organic photoswitches. We have shown experimentally that the coupling of the molecule to the electrodes controls the optical on−off ratio, and theory predicts that low-voltage devices will be very sensitive to photon energy. These ideas pave the way toward tailored molecular-scale optoelectronic devices.

■ ASSOCIATED CONTENT

Supporting Information

The Supporting Information is available free of charge on the ACS Publications website at DOI: 10.1021/acs.nanolett.6b05091.

Experimental setup, additional data and error analysis, temperature-dependent measurements, background theory, polarization dependence, enhancement in gold point-contacts, correlation between optical current and mechanical current (PDF)

■ AUTHOR INFORMATION

Corresponding Author

*E-mail: lv2117@columbia.edu.

ORCID

E-Dean Fung: 0000-0001-6996-0243

Latha Venkataraman: 0000-0002-6957-6089

Notes

The authors declare no competing financial interest.

■ ACKNOWLEDGMENTS

We thank David Reichman, Eran Rabani, and Jeffrey Bokor for useful discussions. This work was supported primarily by the National Science Foundation Grant CHE-1404922. Giacomo Lovat acknowledges support from the Center for Precision Assembly of Superstratic and Superatomic Solids at Columbia University, an NSF MRSEC (award number DMR-1420634).

■ REFERENCES

(1) Galperin, M.; Nitzan, A. *Phys. Chem. Chem. Phys.* **2012**, *14*, 9421−9438.
(2) Aradhya, S. V.; Venkataraman, L. *Nat. Nanotechnol.* **2013**, *8*, 399−410.
(3) Zhang, J. L.; Zhong, J. Q.; Lin, J. D.; Hu, W. P.; Wu, K.; Xu, G. Q.; Wee, A. T. S.; Chen, W. *Chem. Soc. Rev.* **2015**, *44*, 2998−3022.
(4) Dulić, D.; van der Molen, S. J.; Kudernac, T.; Jonkman, H. T.; de Jong, J. J. D.; Bowden, T. N.; van Esch, J.; Feringa, B. L.; van Wees, B. J. *Phys. Rev. Lett.* **2003**, *91*, 207402.
(5) Jauho, A.-P.; Wingreen, N. S.; Meir, Y. *Phys. Rev. B: Condens. Matter Mater. Phys.* **1994**, *50*, 5528−5544.
(6) Kohler, S.; Camalet, S.; Strass, M.; Lehmann, J.; Ingold, G.-L.; Hänggi, P. *Chem. Phys.* **2004**, *296*, 243−249.
(7) Platero, G.; Aguado, R. *Phys. Rep.* **2004**, *395*, 1−157.
(8) Kohler, S.; Lehmann, J.; Hänggi, P. *Phys. Rep.* **2005**, *406*, 379−443.
(9) Dayem, A. H.; Martin, R. J. *Phys. Rev. Lett.* **1962**, *8*, 246−248.
(10) Tien, P. K.; Gordon, J. P. *Phys. Rev.* **1963**, *129*, 647−651.
(11) Pettinger, B.; Ren, B.; Picardi, G.; Schuster, R.; Ertl, G. *Phys. Rev. Lett.* **2004**, *92*, 096101.
(12) Campion, A.; Kambhampati, P. *Chem. Soc. Rev.* **1998**, *27*, 241−250.
(13) Giugni, A.; Torre, B.; Toma, A.; Francardi, M.; Malerba, M.; Alabastri, A.; Zaccaria, R. P.; Stockman, M. I.; Fabrizio, E. D. *Nat. Nanotechnol.* **2013**, *8*, 845−852.
(14) Lal, S.; Link, S.; Halas, N. J. *Nat. Photonics* **2007**, *1*, 641−648.
(15) Ozbay, E. *Science* **2006**, *311*, 189−193.
(16) Zhang, J.; Zhang, L.; Xu, W. *J. Phys. D: Appl. Phys.* **2012**, *45*, 113001.
(17) Lenner, M.; Rácz, P.; Dombi, P.; Farkas, G.; Kroó, N. *Phys. Rev. B: Condens. Matter Mater. Phys.* **2011**, *83*, 205428.
(18) Nguyen, H. Q.; Cutler, P. H.; Feuchtwang, T. E.; Huang, Z. H.; Kuk, Y.; Silverman, P. J.; Lucas, A. A.; Sullivan, T. E. *IEEE Trans. Electron Devices* **1989**, *36*, 2671−2678.
(19) Bragas, A. V.; Landi, S. M.; Martínez, O. E. *Appl. Phys. Lett.* **1998**, *72*, 2075−2077.
(20) Ward, D. R.; Hüser, F.; Pauly, F.; Cuevas, J. C.; Natelson, D. *Nat. Nanotechnol.* **2010**, *5*, 732−736.
(21) Sollner, T. C. L. G.; Goodhue, W. D.; Tannenwald, P. E.; Parker, C. D.; Peck, D. D. *Appl. Phys. Lett.* **1983**, *43*, 588−590.
(22) Ittah, N.; Noy, G.; Yutsis, I.; Selzer, Y. *Nano Lett.* **2009**, *9*, 1615−1620.
(23) Benner, D.; Boneberg, J.; Nürnberger, P.; Waitz, R.; Leiderer, P.; Scheer, E. *Nano Lett.* **2014**, *14*, 5218−5223.
(24) Guhr, D. C.; Rettinger, D.; Boneberg, J.; Erbe, A.; Leiderer, P.; Scheer, E. *Phys. Rev. Lett.* **2007**, *99*, 086801.
(25) Vadai, M.; Nachman, N.; Ben-Zion, M.; Bürkle, M.; Pauly, F.; Cuevas, J. C.; Selzer, Y. *J. Phys. Chem. Lett.* **2013**, *4*, 2811−2816.
(26) Arielly, R.; Ofarim, A.; Noy, G.; Selzer, Y. *Nano Lett.* **2011**, *11*, 2968−2972.
(27) Yoshida, K.; Shibata, K.; Hirakawa, K. *Phys. Rev. Lett.* **2015**, *115*, 138302.
(28) Govorov, A. O.; Zhang, H.; Gun'ko, Y. K. *J. Phys. Chem. C* **2013**, *117*, 16616−16631.
(29) Kornbluth, M.; Nitzan, A.; Seideman, T. *J. Chem. Phys.* **2013**, *138*, 174707.
(30) Sundararaman, R.; Narang, P.; Jermyn, A. S.; Goddard, W. A., III; Atwater, H. A. *Nat. Commun.* **2014**, *5*, 5788.
(31) Bernardi, M.; Mustafa, J.; Neaton, J. B.; Louie, S. G. *Nat. Commun.* **2015**, *6*, 7044.
(32) Banerjee, P.; Conklin, D.; Nanayakkara, S.; Park, T.-H.; Therien, M. J.; Bonnell, D. A. *ACS Nano* **2010**, *4*, 1019−1025.
(33) Pal, P. P.; Jiang, N.; Sonntag, M. D.; Chiang, N.; Foley, E. T.; Hersam, M. C.; Van Duyne, R. P.; Seideman, T. *J. Phys. Chem. Lett.* **2015**, *6*, 4210−4218.
(34) Vadai, M.; Selzer, Y. *J. Phys. Chem. C* **2016**, *120*, 21063−21068.
(35) Tan, S. F.; Wu, L.; Yang, J. K. W.; Bai, P.; Bosman, M.; Nijhuis, C. A. *Science* **2014**, *343*, 1496−1499.
(36) Thon, A.; Merschdorf, M.; Pfeiffer, W.; Klamroth, T.; Saalfrank, P.; Diesing, D. *Appl. Phys. A: Mater. Sci. Process.* **2004**, *78*, 189−199.
(37) Wu, S. W.; Ogawa, N.; Ho, W. *Science* **2006**, *312*, 1362−1365.
(38) Wu, S. W.; Ho, W. *Phys. Rev. B: Condens. Matter Mater. Phys.* **2010**, *82*, 085444.
(39) Quek, S. Y.; Kamenetska, M.; Steigerwald, M. L.; Choi, H. J.; Louie, S. G.; Hybertsen, M. S.; Neaton, J. B.; Venkataraman, L. *Nat. Nanotechnol.* **2009**, *4*, 230−234.
(40) Adak, O.; Korytár, R.; Joe, A. Y.; Evers, F.; Venkataraman, L. *Nano Lett.* **2015**, *15*, 3716−3722.
(41) Xu, B.; Tao, N. J. *Science* **2003**, *301*, 1221−1223.

DOI: 10.1021/acs.nanolett.6b05091
Nano Lett. 2017, 17, 1255−1261

(42) Kotiuga, M.; Darancet, P.; Arroyo, C. R.; Venkataraman, L.; Neaton, J. B. *Nano Lett.* **2015**, *15*, 4498−4503.
(43) Tsutsui, M.; Taniguchi, M.; Kawai, T. *Nano Lett.* **2008**, *8*, 3293−3297.
(44) Huang, Z.; Chen, F.; D'agosta, R.; Bennett, P. A.; Di Ventra, M.; Tao, N. *Nat. Nanotechnol.* **2007**, *2*, 698−703.
(45) Widawsky, J. R.; Darancet, P.; Neaton, J. B.; Venkataraman, L. *Nano Lett.* **2012**, *12*, 354−358.
(46) Nitzan, A.; Ratner, M. A. *Science* **2003**, *300*, 1384−1389.
(47) Peskin, U. *J. Phys. B: At., Mol. Opt. Phys.* **2010**, *43*, 153001.
(48) Wagner, M.; Zwerger, W. *Phys. Rev. B: Condens. Matter Mater. Phys.* **1997**, *55*, R10217−R10220.
(49) Hou, S.; Zhang, J.; Li, R.; Ning, J.; Han, R.; Shen, Z.; Zhao, X.; Xue, Z.; Wu, Q. *Nanotechnology* **2005**, *16*, 239.
(50) Pérez-Jiménez, Á. J. *J. Phys. Chem. B* **2005**, *109*, 10052−10060.
(51) Kaganov, M. I.; Lifshitz, I. M.; Tanatarov, L. V. *Sov. Phys. J. Exp. Theor. Phys.* **1957**, *4*, 232.
(52) Pines, D.; Nozières, P. Response and Correlation in Homogeneous Electron Systems. *Normal Fermi liquids*; W.A. Benjamin: New York, 1966; Vol. *1*, pp 202−269.
(53) Fann, W. S.; Storz, R.; Tom, H. W. K.; Bokor, J. *Phys. Rev. B: Condens. Matter Mater. Phys.* **1992**, *46*, 13592−13595.
(54) Sun, C.-K.; Vallée, F.; Acioli, L. H.; Ippen, E. P.; Fujimoto, J. G. *Phys. Rev. B: Condens. Matter Mater. Phys.* **1994**, *50*, 15337−15348.
(55) Cvetko, D.; Fratesi, G.; Kladnik, G.; Cossaro, A.; Brivio, G. P.; Venkataraman, L.; Morgante, A. *Phys. Chem. Chem. Phys.* **2016**, *18*, 22140−22145.
(56) Quek, S. Y.; Venkataraman, L.; Choi, H. J.; Louie, S. G.; Hybertsen, M. S.; Neaton, J. B. *Nano Lett.* **2007**, *7*, 3477−3482.
(57) Sze, S. M.; Moll, J. L.; Sugano, T. *Solid-State Electron.* **1964**, *7*, 509−523.
(58) Kanter, H. *Phys. Rev. B* **1970**, *1*, 522−536.
(59) Ashcroft, N. W.; Mermin, N. D. The Sommerfeld Theory of Metals. *Solid State Physics*; Brooks/Cole Thomson Learning: New York, 1976; pp 29−56.
(60) Olmon, R. L.; Slovick, B.; Johnson, T. W.; Shelton, D.; Oh, S.-H.; Boreman, G. D.; Raschke, M. B. *Phys. Rev. B: Condens. Matter Mater. Phys.* **2012**, *86*, 235147.
(61) Huber, R.; Koch, M.; Feldmann, J. *Appl. Phys. Lett.* **1998**, *73*, 2521−2523.
(62) Grafström, S.; Schuller, P.; Kowalski, J.; Neumann, R. *J. Appl. Phys.* **1998**, *83*, 3453−3460.

DOI: 10.1021/acs.nanolett.6b05091
Nano Lett. 2017, 17, 1255−1261